Chapter 4

Influence of SiC content to control the morphology of in-situ synthesized ZrB_2-SiC composite through a single-step reduction process

4. 1 Introduction

The present chapter focuses on the influence of SiC content on the morphology and microstructure of in-situ synthesized ZrB_2-SiC composite for ultra-high temperature applications. The ZrB_2-SiC composite was synthesized with controlled microstructure by optimizing the mole content of raw powders ZrO_2, B_4C, and Si at lower synthesis temperatures through a single-step reduction process. The synthesis of the ZrB_2-SiC composite was affected by the variation in mole content of the starting reactant and calcination temperature. The chemical reaction that occurs between the raw materials can be expressed in (4.1) as follows:

$$2ZrO_2(s) + 1.5B_4C(s) + 0.5Si(s) \rightarrow 2ZrB_2(s) + 0.5SiC(s) + B_2O_3(g, l) + CO(g) \qquad (4.1)$$

A detailed explanation of the specifications for the starting material is already provided in Chapter 3. The starting ZrO_2, B_4C, and Si raw materials were dry-mixed in a different mole content in high energy ball milling (FRITSCH pulveristte 5) at 300 rpm for 2h using a ZrO_2 ball as a grinding medium (mentioned in Table 4.1). Adjusting the initial composite is essential for introducing variations in the SiC components within the final composite. The ratio of powder to balls is 1:10 during high-energy ball milling. Subsequently, a uniaxial hydraulic pressing machine isostatically pressed the raw mixed powder at 12 MPa pressure. The sample diameter and thickness were 10 mm and 5 mm, respectively, drying at 100°C for 24 h. The pressed samples were placed in a graphite crucible positioned in a tube furnace, maintaining a moderate vacuum (10^{-2} torr) backfilled by argon. The sample was heat-treated at 1300-1600°C for 3h and at a continuous rate of 5 °C /min. The molar ratio of ZrO_2:B_4C: Si was increased

from 2:1.5:0.5 to 2:1.67:1.34 at 1300-1500°C, resulting in increased SiC content and reduced average grain size.

Table 4.1 The composition of raw materials ZrO_2, B_4C, and Si for the synthesis of ZrB_2-SiC composite

Sample name	Mole content			Note
	ZrO_2	B_4C	Si	
S1	2	1.5	0.5	Stoichiometric reaction (6)
S2	2	1.5	0.75	Increase 0.25 mole of Si
S3	2	1.67	1	Increase 0.17 mole of B_4C and 0.5 mole of Si
S4	2	1.67	1.34	Increase 0.17 mole of B_4C and 0.84 mole of Si

In this chapter, the phase analysis, microstructure, and XPS analysis determine the composite. The Rietveld refinement method (RRM) calculates the wt % of the ZrB_2 and SiC phases in the final samples.

4. 2 Result and discussion

4.2.1 Thermodynamic calculation

The thermodynamic data of reactions define the feasibility of reactions at elevated temperatures. The reaction (4.1) was favorable at 930°C under ambient pressure (P = 1.01325 bar) calculated by using FactSage thermochemical software [176]. The Gibbs phase energy of the reaction (4.1) is negative at 930°C, and it diminishes with increasing the synthesis temperature. As a result, the ZrB_2-SiC composite was synthesized at a relatively lower temperature. But carbon, B_2O_3(l), and SiO_2(s) phases were also present at 930°C ambient pressure.

Further increasing the temperature up to 1520°C under ambient pressure, the formation of 2 moles of ZrB_2, 0.5 moles of SiC, 1 mole of B_2O_3(l), and 1 mole of CO(g) takes place in

ZrB_2-SiC composite. Accordingly, in a calculation, 2 moles of ZrO_2 were converted into 2 moles of ZrB_2(s), and residual B_4C and Si produced the SiC phase. The mole content of SiC was changed by varying the molar ratio of ZrO_2:B_4C: Si at 1520°C at 1.01325 bar ambient pressure, shown in Table 4.2. The thermodynamic calculation confirms that the synthesis of the ZrB_2-SiC composite can occur by the optimum molar ratio of the starting reactant at the appropriate temperature.

Table 4.2 Variation of ZrB_2, SiC, and other phases with the different ZrO_2, B_4C, and Si mole content at 1520°C and under ambient pressure (P = 1.01325 bar).

Sample name	Mole content			Other phase
	ZrB_2(s)	SiC(s)	B_2O_3(l)	
S1	2	0.499	0.994	0.00633 Graphite
S2	2	0.664	0.994	0.08 SiO_2
S3	2	1	1.33	0.06 C, 0.003 B_4C
S4	2	1.665	1.33	0.005 SiO_2, 0.005 B_4C

4.2.2 Effect of temperature on the synthesis of ZrB_2-SiC composite

The XRD pattern of heat-treated ZrB_2-SiC powder obtained from S1 in Fig. 4.1. The XRD pattern indicates that S1 contains a high amount of untreated ZrO_2 (JCPDS NO 07-0343), and B_4C (JCPDS NO 75-0424) at 1300°C along with a few amounts of ZrB_2 (JCPDS NO 75-1050) and SiC (JCPDS NO 29-1129) phase. The ZrB_2 and SiC formations occur at 1300°C and above only. Reaction (4.1) is feasible at 930°C, but Si reacted with C of B_4C only to form SiC at 1300°C. The released boron reacted with ZrO_2, forming ZrB_2, but a temperature of 2227°C is required to complete the reaction [177]. As the temperature increases to 1400°C, the ZrO_2 phase and other impurities decrease, and the ZrB_2 phase is enhanced along with the SiC phase.

Interestingly, pure ZrB_2-SiC phases occurred at 1500°C. With a further increase in temperature, the XRD spectrum revealed no presence of the B_2O_3 phase.

The Rietveld refinement method calculated the relative phase content of ZrB_2 and SiC. At 1300°C, the relative wt% of ZrB_2, SiC, and ZrO_2 was about 41wt %, 6.1 wt %, and 52.9 wt %, respectively, along with other impurities. Furthermore, on increasing the temperature to 1500°C, the relative content of SiC increased rapidly up to 7 wt%, and the ZrO_2 phase disappeared. The wt% of SiC is very close to the theoretical fraction of the reaction (4.1). The pure ZrB_2-SiC phase was obtained at 1500°C, lower than 1520°C (thermochemical stable temperature by software). It may occur due to a moderate vacuum backfill with an argon supply. The high vacuum pressure and argon supply decreased the saturation temperature of reactions.

Another essential point to be considered is that the argon atmosphere suppressed the vaporization of B_2O_3. As a result, no extra amount of B_4C was required to reduce ZrO_2 to synthesize the ZrB_2-SiC composite completely. Surface oxides like B_2O_3 are responsible for grain coarsening by evaporation-condensation kinetics with increasing temperature, which hinders the composite's densification and is thus responsible for the degradation of mechanical characteristics.

Many researchers have reported that the 20 wt% of SiC provided better densification, ablation, and oxidation resistance than pure ZrB_2 [174,178,179]. Thus, to see the advantage of SiC, the mole content of the reactant varied to improve the densification and mechanical properties of ZrB_2-based ceramic [180].

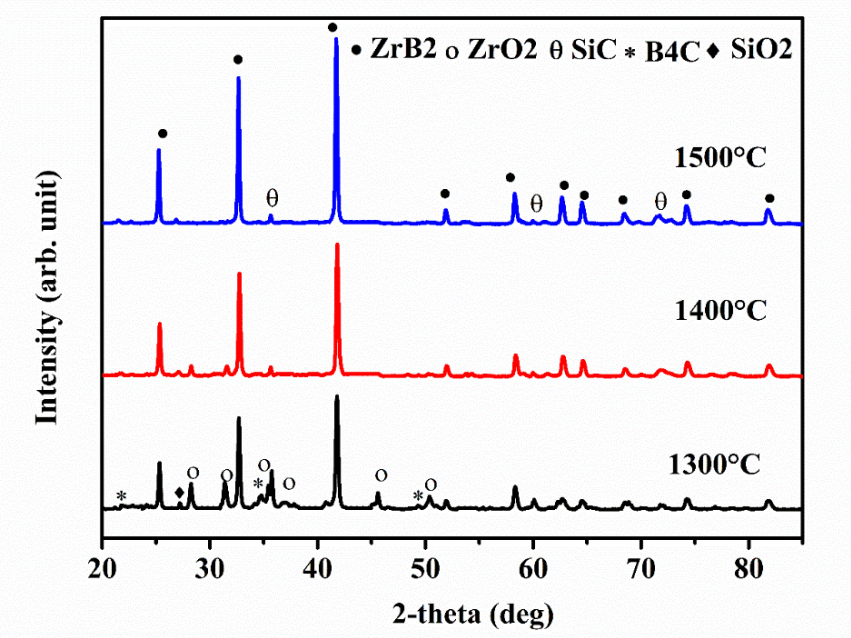

Fig. 4.1 X-ray diffraction pattern of the sample S1 (stoichiometric proportion) at different temperatures

The XRD pattern of S4 after thermal treatment at different temperature ranges in Fig. 4.2. A large amount of SiO_2 impurity and unreacted ZrO_2 and B_4C occur at 1300°C. This synthesis temperature was insufficient for converting ZrO_2 and B_4C into ZrB_2. At 1400°C, the ZrB_2 and SiC phases increase, whereas the ZrO_2 phase decreases. In the X-ray diffraction pattern of the heat-treated sample at 1400°C, no carbon peak occurs due to the presence of B_4C and SiC phases and the disordered structure of sp^3 carbon. Further on increasing the synthesis temperature to 1500°C, the residual reactant converted into ZrB_2, and only ZrB_2 and SiC phases appeared in the XRD spectrum. The amount of SiC phase present in the final composition was determined by the Rietveld refinement analysis, about 18 wt%, which has excellent oxidation resistance at higher temperatures compared to the 7 wt % sample [181,182]. In general, the addition of SiC improves sinterability and restricts the grain growth of borides.

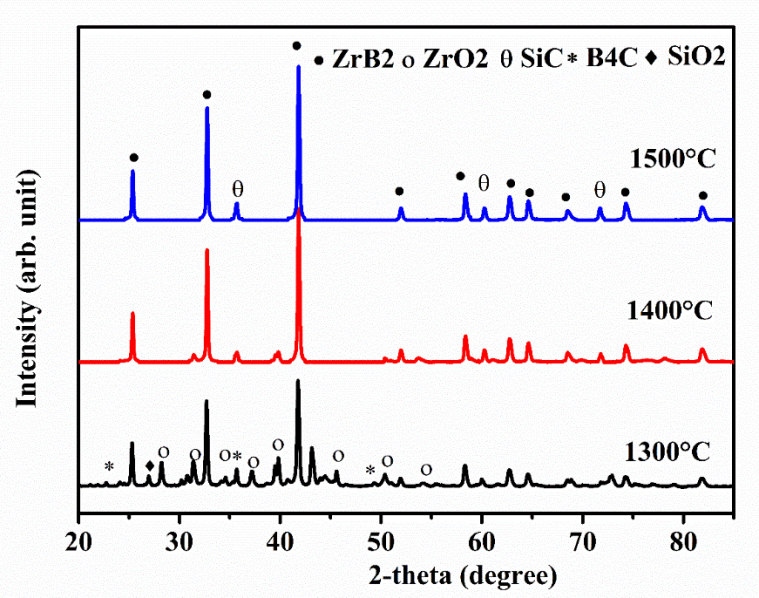

Fig. 4.2 X-ray diffraction patterns of the sample S4 at various temperatures

SEM image for sample S4, at different temperature ranges of 1400°C and 1600°C, is shown in Fig. 4.3 (a) and Fig. 4.3 (b), respectively. When sample S4 is heat treated at 1400°C, the presence of oxide impurities hinders the densification process. Further increasing the temperature from 1400°C to 1600°C, densification happens in the final composite. The Oxides, like ZrO_2, disappear, and densification occurs when facilitated at high temperatures.

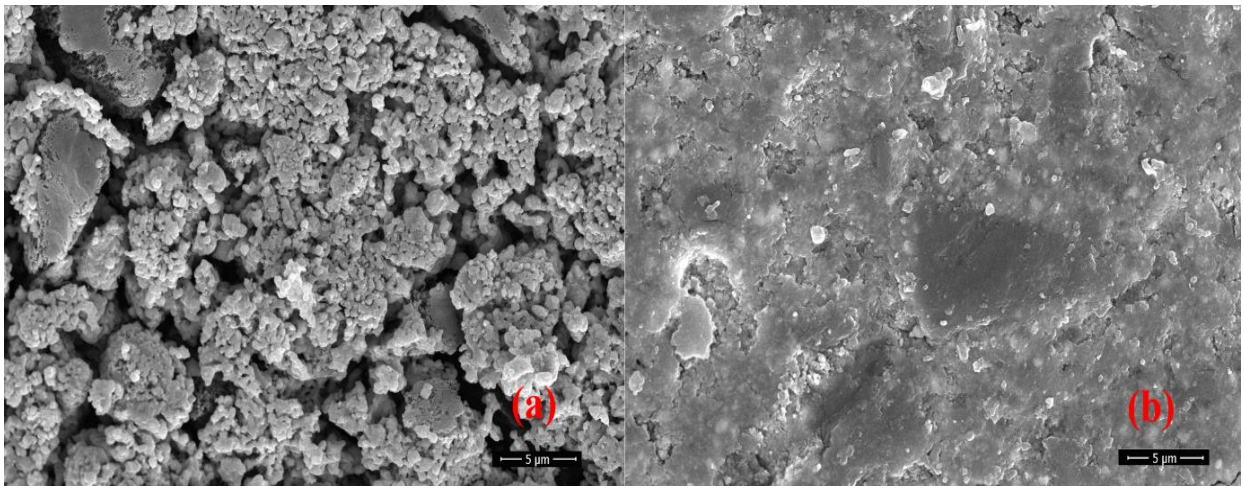

Fig. 4.3 SEM image of thermally treated sample S4 at two distinct calcination temperatures: (a) 1400°C and (b) 1600°C

4.2.3 Effect of molar ratio of ZrO_2:B_4C: Si on the ZrB_2-SiC composite

The XRD pattern of S1, S2, S3, and S4 powder at 1500°C shown in Fig. 4.4. The sample S1 (stoichiometric ratio) has a minor amount of SiC phase in the ZrB_2-SiC composite. Fig. 4. 5 shows the phase composition of ZrB_2 and SiC in a bar diagram. The bar diagram shows the SiC content increased by increasing the mole content of ZrO_2, B_4C, and Si for samples S1 to S4. When the molar ratio of ZrO_2:B_4C: Si (sample S2) was 2:1.5:0.75, a minor amount of ZrO_2 impurity was present due to deficiency of B_4C along with ZrB_2 and SiC phase. Considering the importance of Si, the molar ratio of ZrO_2:B_4C: Si was increased from 2:1.5:0.75 (sample S2) to 2:1.67:1 (sample S3), leaving a minor impurity of ZrO_2 and C. The SiC content increased from 9 wt % to 14 wt % for S2 and S3, respectively, while the theoretical value calculated from the FactSage software is 10.619 wt % and 15.094 9 wt %. Finally, for sample S4 (ZrO_2:B_4C: Si- 2:1.67:1.34), the SiC amount increased from 14 wt% to 18 wt% along with the ZrB_2 phase. Rietveld refinement method (RRM) is employed to conduct quantitative phase analysis. The wt % The actual content of SiC was less than the calculated value due to the volatilization of Si or intermediate borosilicate phase formation during the whole synthesis. The argon atmosphere plays a crucial role in suppressing the vaporization of intermediate products like B_2O_3, trapped in pores and channels of precursors at a higher temperature. The trapped B_2O_3 products converted into ZrB_2 after reduction with ZrO_2. Thus, among the various compositions, the S4 composition provided an impurity-free ZrB_2-SiC composite by ultimately converting the reactant at a relatively lower synthesis temperature.

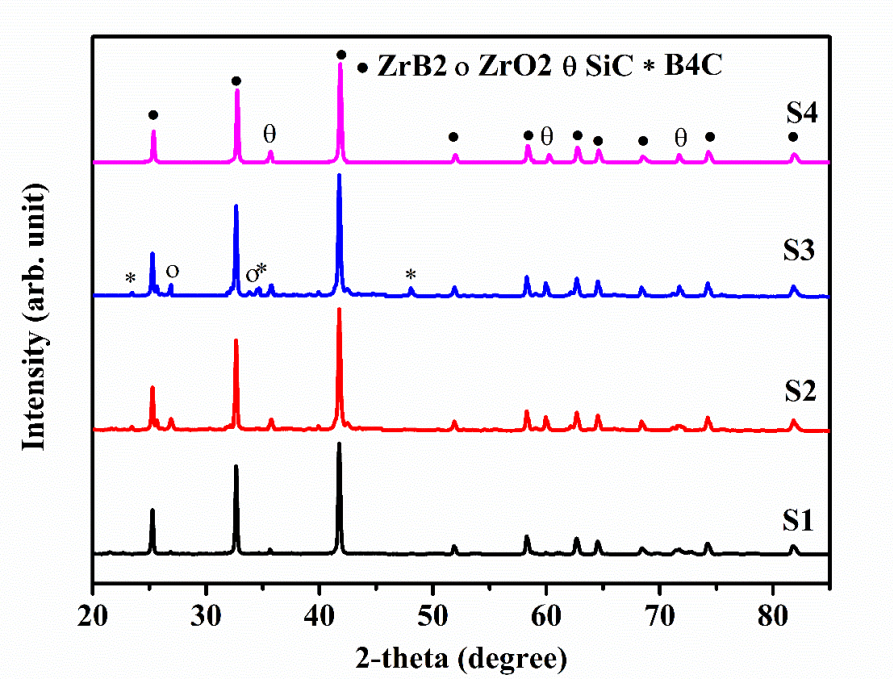

Fig. 4.4 X-ray diffraction pattern of synthesized S1-S4 samples at 1500°C

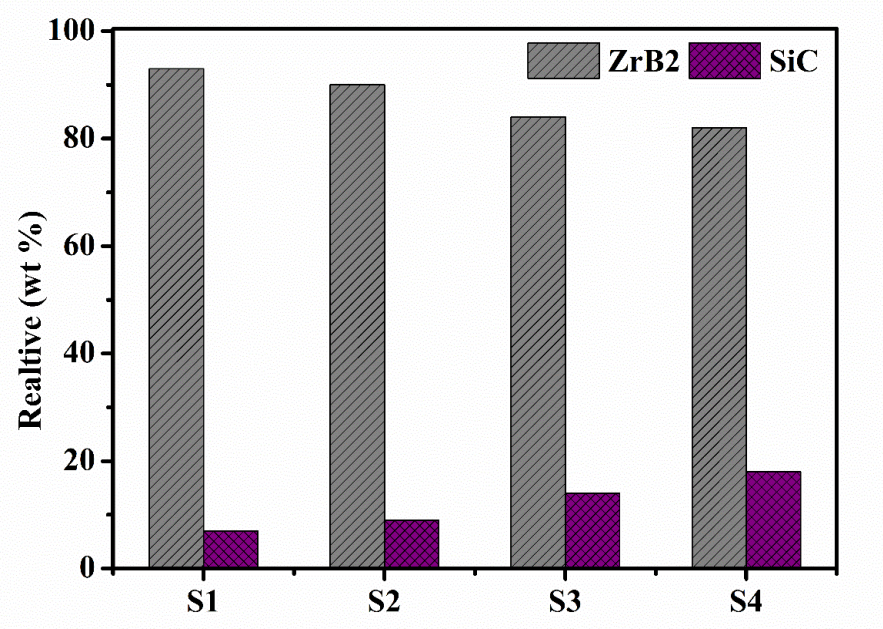

Fig. 4.5 Phase compositions of ZrB_2 and SiC for various samples

The XPS analysis was performed on the clean surface of sample S4, shown in Fig. 4.6. (a)-(f). Fig. 4.6 (a) indicated the XPS survey spectrum of the sample. It consists of significant peaks of B 1s, Zr 3d, Si 2p, C 1s, and O 1s mentioned in Table 4 and minor peaks of Zr 3s, Zr $3p_{1/2}$ Zr $3p_{3/2}$, Si 2s, Zr 4s, and O 2s. The oxygen spectra indicated the oxide present on the surface of the sample. Fig 4.6 (b) illustrates the valence band spectra for the sample near the

FL. The FL cut-off (Fermi edge) corresponds to "0 eV" on the BE scale, indicating that the FL is aligned between the sample and the spectrometer, demonstrating that good electrical contact with the instrument has been established. Thus, all BE values computed this way are expressed for the FL [183]. Fig. 4.6 (c) revealed the presence of the B 1s spectrum at 187.8± 0.1 eV due to the existence of B-Zr corresponding to the ZrB_2 compound [184]. The Zr 3d peaks are fit into four main components. The spin-orbit splitting of Zr 3d $_{5/2}$ and Zr 3d $_{3/2}$ peak at 182.6 ± 0.1 eV and 184.9 ± 0.1 eV is associated with Zr-O bonds related to ZrO_2. The Zr 3d $_{5/2}$ and Zr 3d $_{3/2}$ peak at 178.6 ± 0.1 eV and 180.9 ± 0.1 eV related to Zr-B bonds, corresponding to ZrB_2 [184,185]. The presence of the O 1s spectrum fits into two components shown in Fig 4.6 (d). The binding energy exhibited at 531.7 ± 0.1 eV and 532.2 ± 0.1 are related to O-Zr and O-Si bonds [186] because of the ZrO_2 and SiO_2 compounds in the ZrB_2-SiC composite. The XPS is highly sensitive to the surface binding energy, and the ZrB_2 is highly sensitive to oxidation in amphoteric oxygen to form oxide. The XPS is the most common technique for determining chemical bonding and functional groups on the surfaces and interfaces, and it cannot select the complete quantity of Zr, B, Si, and C present in the ZrB_2-SiC composite. Fig 4.6 (e) shows that the Si 2p spectrum related to Si-C bonds at 99.7± 0.1 eV and Si-O bonds at 101.8 ± 0.1 eV [187], owing to the presence of SiO_2 on the surface of the composite. The fitted C 1s peak at 282 ± 0.1 eV corresponds to C-Si bonds shown in Fig. 4.6 (f). The peak position located at 284.5 ± 0.1 eV is related to the C-C (sp^3) bond, attributed to the C 1s spectra of an adventitious carbon (AdC) layer, generally present on all air-exposed samples. AdC is a compound of unknown origin and composition, not an inherent part of the sample, and does not make proper electrical contact with the analyzed sample [188,189]. For non-conducting materials, charge reference is required because they tend to gain positive potential during measurement, which decreases the photoelectron kinetic energy and, as a result, causes the recorded binding energies to appear to shift upwards [183]. Siegbahn et al. [190] suggested using the C 1s peak of

adventitious carbon for charge referencing, and it has been one of the most common methods reported in various investigations [191,192]. However, aligning the spectra to the C 1s peak of adventitious carbon is unreliable. It may lead to unphysical results owing to its alarmingly wide binding energy range from 284.08 – 286.74 eV [193]. Furthermore, by the XRD and further analysis (SEM and TEM), it can be concluded that there is no internal phase formation of carbon, confirming the appearance of the pure crystalline phase of ZrB_2.

Table 4.3 XPS spectra for in-situ synthesized ZrB_2-SiC composite

Element peak	Binding energy (± 0.1) eV	Chemical Bond	FWHM (± 0.05) eV
B 1s	187.8	B-Zr	0.9
Zr 3d 3/2	184.9	Zr-O	1.6
Zr 3d 5/2	182.5	Zr-O	1.8
Zr 3d 3/2	180.9	Zr-B	1.3
Zr 3d 5/2	178.6	Zr-B	1.2
Si 2p	99.7	Si-C	1.8
Si 2p	101.8	Si-O	2.3
O 1s	531.7	O-Zr	2.3
O 1s	532.2	O-Si	2.6
C 1s	282	C-Si	1.8
C 1s (sp^3)	284.5	C-C	1.4

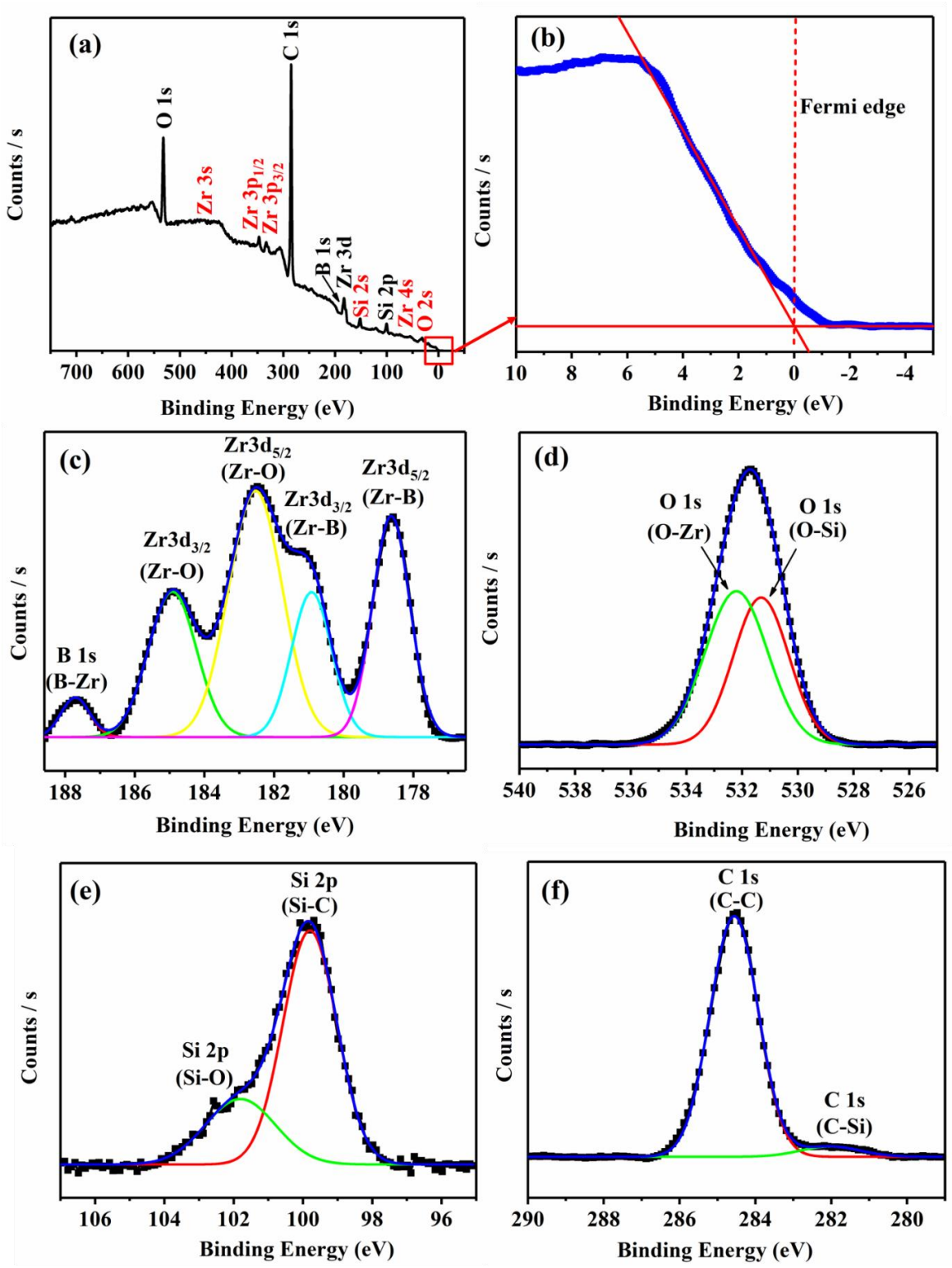

Fig. 4.6 XPS analysis for in situ synthesized ZrB_2-SiC composite (S4) at 1400°C (a) Full range XPS (b) Valance band spectra in the vicinity of the FL of the sample (c) Zr 3d and B 1s (d) O 1s (e) Si 2p (f) C1s

4.2.4 Influence of ZrO_2:B_4C: Si molar ratio on the microstructure of ZrB_2-SiC composite

The morphology and microstructure of thermally treated ZrB_2-SiC composite (S1) at 1400°C were analyzed using SEM. The elongated shaped grain (Φ 0.5 µm, 1- 1.5µm), nearly granular particle (Φ 0.1-0.5 µm), and numerous tiny particles in Fig. 4.7 (a). Fig. 4.7 (b), (c), and (d) show the spot EDS analysis of the SEM image shown in Fig. 4.7 (a). The EDS analysis identifies the elements present in the composite. Spot 1 (granular cluster), spot 2 (elongated grain), and spot 3 (small particle) mainly consist of Si and carbon elements along with Zr and boron elements. The EDS analysis confirms the present of Zr, B, Si and C element in the final composite. A similar type of structure is formed by Cao et al. [194]. The elongated ZrB_2 was created due to its inherent crystallography property and bond energy. Also, the growing behavior of ZrB_2 at various planes is due to its bond energy. The higher energy plane tends to grow faster than other planes and finally disappears. The bond energy for B-Zr is lower than that of B-B but higher than Zr-Zr [195]. As a result, the {110} plane family with B-Zr bonds tends to grow rapidly and finally disappears. The (001) plane with Zr-Zr bonds is maintained in the final structure due to its slowest growth rate. Apart from the factors mentioned above, for the growth of ZrB_2 along the preferred [001] direction, some other factors should also be considered [196].

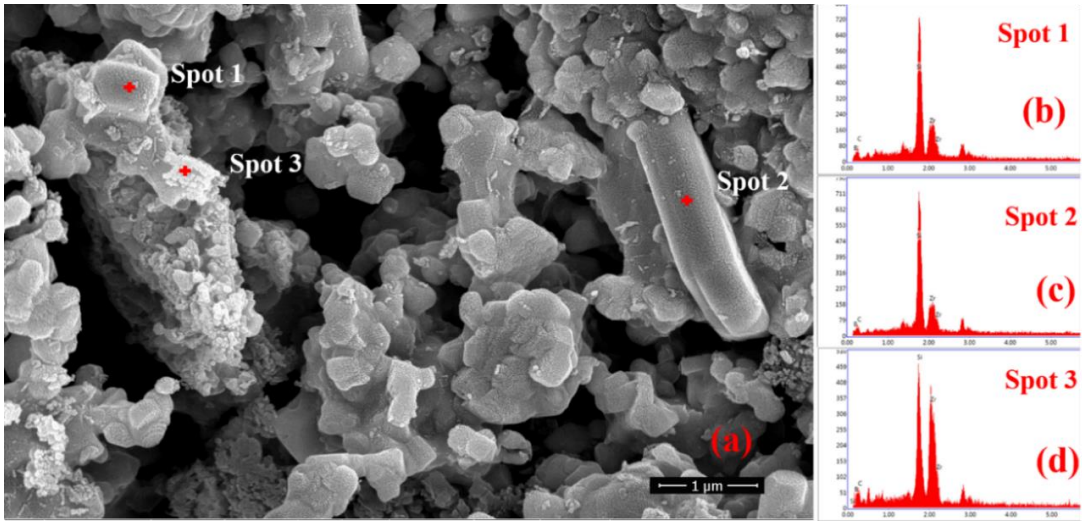

Fig. 4.7 SEM image (a) and EDS spectra (b, c, d) of ZrB_2-SiC (S1) composite at 1400 °C

The formation of B_2O_3 during the intermediate stage is also responsible for the anisotropic growth of ZrB_2. The molten form of this B_2O_3 might act as a "reaction cell" and decrease the nucleation point for ZrB_2, resulting in the migration of atoms during crystalline growth. In comparison, the vapor form of B_2O_3 evolved due to high-temperature forms of ZrB_2 nuclei after interacting with a solid phase of ZrO_2-C. In addition, continuous argon flow is also responsible for the preferential growth of ZrB_2 by diminishing the supersaturation of B_2O_3. In ZrB_2- SiC composite, the elongated shaped ZrB_2 particle is smaller than the single-phase ZrB_2 particle (Φ 1-2 μm, 3-15 μm) [196]. The incorporation of SiC acts as a grain growth inhibitor [197]. The microstructure of the lower SiC content composite shows a porous structure. The content of tiny SiC particles is increased by varying the starting precursor's mole content, resulting in the densification and homogeneous structure.

Fig. 4.8 (a)-(d) shows the morphology and phase composition of sample S4 with an appropriate amount of SiC content at 1400°C. Fig. 4.8 (a) contains three different structures: columnar or elongated shape, granular particles, and tiny nanoparticles. The distribution of the particles is homogeneous throughout the whole composition. Fig. 4.8 (b) shows the distribution of small particles (20-50 nm) is homogeneous. The ZrB_2 grew into an immature large columnar and elongated structure when the temperature increased. The size of ZrB_2 is reduced with SiC addition due to the pinning effect by tiny SiC particles on grain boundaries, which act as grain growth inhibitors that restrict grain boundary mobility during heating[198–200]. Fig. 4.8 (c) and Fig. 4.8 (d) show the EDS analysis of the sample S4. Fig. 4.8 (c) detects the present Zr, C, B, and Si elements. Similarly, Fig. 4.8 (d) contains mainly Si and C elements.

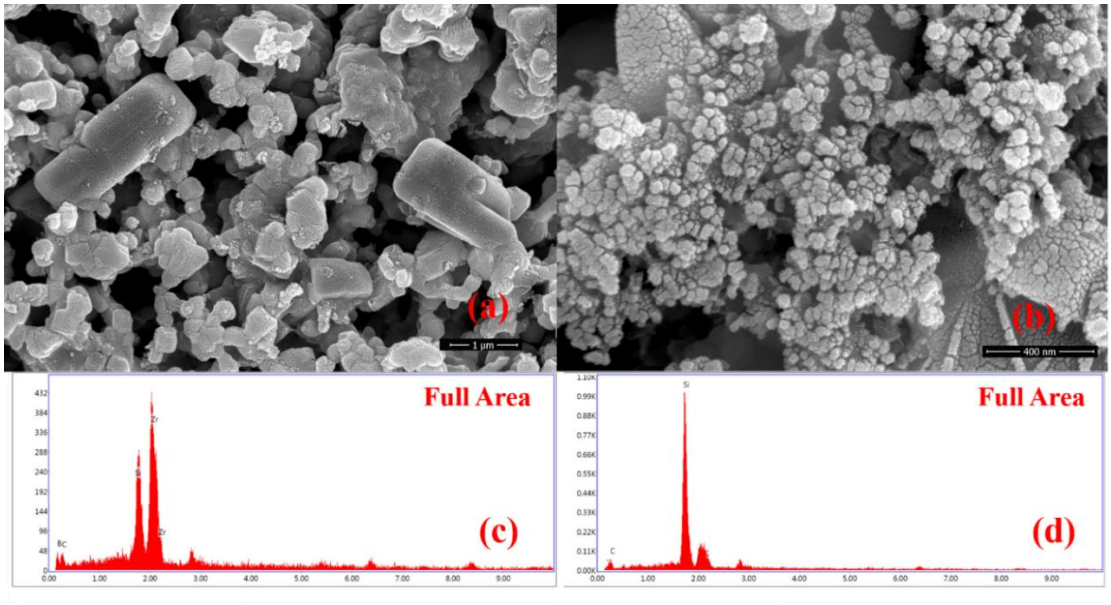

Fig. 4.8 SEM image (a)-(b) and EDS spectra (b)-(c) of ZrB_2-SiC (S4) composite at 1400 °C

Fig. 4.9 (a) and Fig. 4.9 (b) illustrate the morphology and densification of samples S1 and S4, respectively, with an appropriate amount of SiC content at 1600°C. It is observed in Fig. 4.9 (b) for sample S4 that the particle size is reduced compared to Fig. 4.9 (a) for sample S1. Sample S4 has a uniform microstructure due to grain SiC acting as a grain growth inhibitor. As mentioned in the literature [197], with increasing Si content, the particle size of ZrB_2 decreased, leading to a uniform and fine microstructure.

EDS analysis illustrates the elemental composition (area) and mapping of S4 in Fig. 4.9 (b). The mapping of S4 confirmed the homogeneous destitution of Zr, B, C, and Si in the ZrB_2-SiC composite. The SEM microstructure and TEM imaging confirmed that the SiC tiny particle, which controlled the microstructure, morphology, and densification of the ZrB_2-SiC composite.

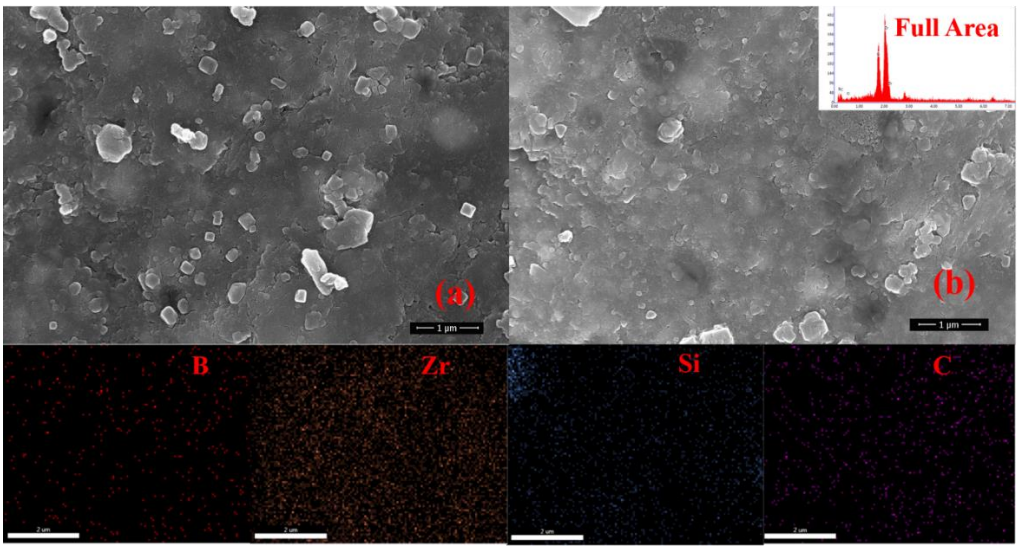

Fig. 4.9 SEM image (a) S1 and (b) S4 with EDS mapping of sample S4 at 1600 °C

The transmission electron microscopic of ZrB_2-SiC powder is illustrated in Fig. 4.10 (a)-(d). The TEM imaging of sample S4 revealed that tiny particles (20 nm-50 nm) were dispersed uniformly along the grain boundaries of well-grown elongated and nearly granular particles (200 nm-500 nm), as shown in Fig. 4.10 (a). Fig. 4.10 (b) illustrates a tiny layer of homogeneously dispersed particles on the nearly spherical surface (80 nm). Fig. 4.10 (c) showed the HRTEM of the red rectangle area indicated in Fig. 4.10 (a). The HRTEM image revealed the single-crystalline nature of the particles, and the Fast Fourier Transform (FFT) pattern shows the lattice imaging along the zone axis [010]. The interplanar spacing between the lattice fringes of 0.352 nm and 0.216 nm matched with the d-spacing of (001) and (101) crystal planes of ZrB_2 (JCPDS NO 75-1050), respectively. The cross product of the direction of crystallographic planes (001) and (101) gives the zone axis [010]. The cross-lattice fringes shown in Fig. 4.10 (d) with the interplanar spacing of 0.252 nm and 0.218 nm corresponding to (111) and (200) planes, respectively, are determined by the FFT pattern of HRTEM. This planer spacing is consistent with the d-spacing of the SiC phase (JCPDS NO 29-1129). Therefore, it can be seen that the tiny particles of SiC were uniformly distributed along the grain boundaries of ZrB_2 particles.

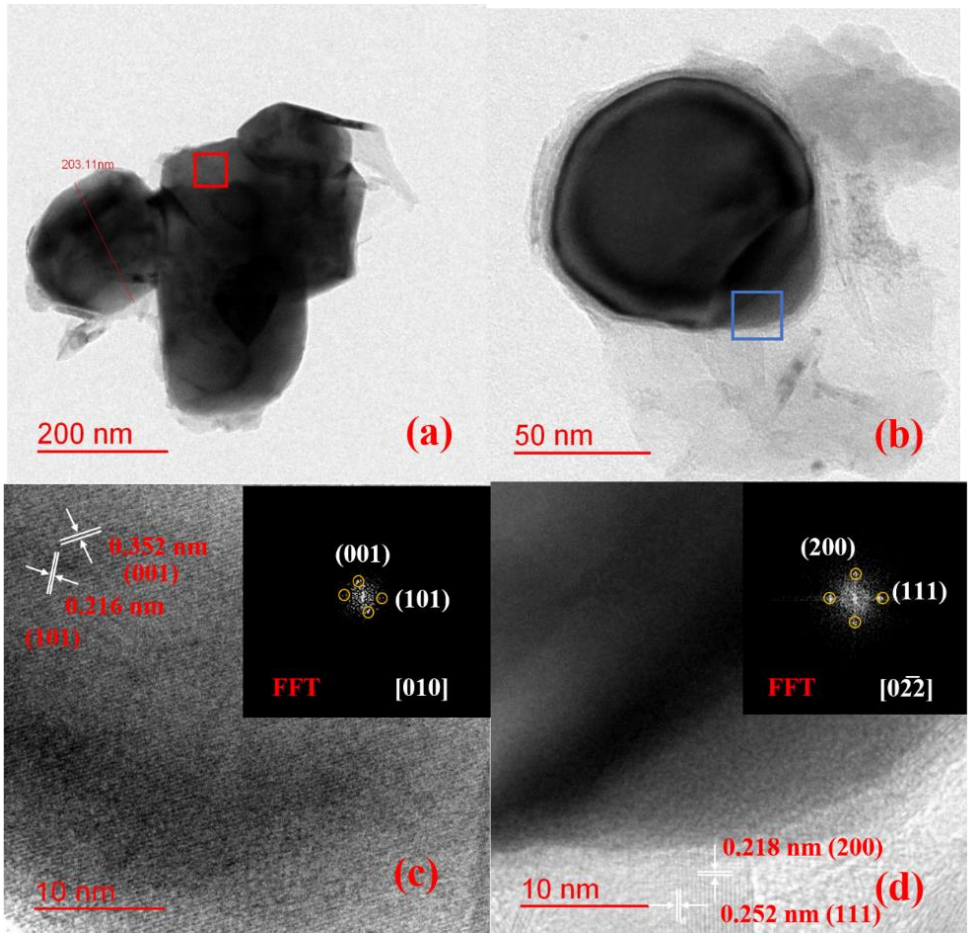

Fig. 4.10 (a) and (b) TEM images of ZrB_2-SiC at 1400 °C, (c) and (d) HRTEM of ZrB_2 and SiC, respectively

4. 3 Conclusion of the chapter

In this study, the influence of SiC content on the morphology and microstructure of in-situ synthesized ZrB_2-SiC composite using ZrO_2, B_4C, and Si via a single-step reduction process under an argon atmosphere. The XRD analysis revealed that the reaction (4.1) in the stoichiometric ratio provided an oxide-free ZrB_2-SiC composite at 1500°C under an argon atmosphere. The argon atmosphere suppressed the vaporization of intermediate products like B_2O_3, which further converts into ZrB_2-SiC, containing about 7 wt % of SiC. Thus, the molar ratio of ZrO_2:B_4C: Si was increased from 2:1.5:0.5 to 2:1.67:1.34, resulting in the amount of SiC being raised to 18 wt % in the ZrB_2-SiC composite. With the significant increase in the wt% of SiC from 7 to 18, the formation of the SiC layer inhibited the grain growth of ZrB_2

particles [197]. As a result, the pinning effect on the grain boundaries increased the densification of the ZrB_2-SiC composite.

Furthermore, the microstructure and morphology of the ZrB_2-SiC composite showcased that the tiny particles (20-50 nm) were distributed on the elongated shaped (Φ 0.5 µm, 1-1.5 µm) and granulation (Φ 0.1-0.5 µm) of particles. The feasibility of the reaction for the synthesis of ZrB_2-SiC composite was established by thermodynamic calculation and experimental results. The composite was synthesized at a comparatively lower temperature due to maintaining a moderate vacuum backfilled by argon.

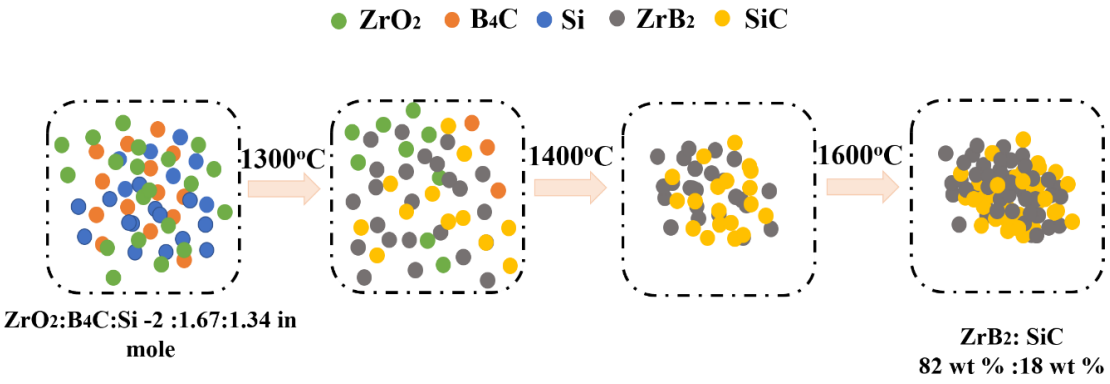

Fig. 4.11 The schematic representation of the possible formation mechanism of ZrB_2-SiC composite with processing temperature and mole content of starting reactant.